

 Open access • Journal Article • DOI:10.1021/ACS.JPROTEOME.6B00753

Robust, Sensitive, and Automated Phosphopeptide Enrichment Optimized for Low Sample Amounts Applied to Primary Hippocampal Neurons — [Source link](#)





Harm Post, Renske Penning, Martin Fitzpatrick, Luc Garrigues ...+5 more authors

Institutions: Utrecht University

Published on: 03 Feb 2017 - Journal of Proteome Research (American Chemical Society)

Related papers:

- [MaxQuant enables high peptide identification rates, individualized p.p.b.-range mass accuracies and proteome-wide protein quantification.](#)
- [Off-Line High-pH Reversed-Phase Fractionation for In-Depth Phosphoproteomics](#)
- [Reversed-phase chromatography with multiple fraction concatenation strategy for proteome profiling of human MCF10A cells](#)
- [The Perseus computational platform for comprehensive analysis of \(prote\)omics data.](#)
- [High-throughput phosphoproteomics reveals in vivo insulin signaling dynamics](#)

Share this paper:    

View more about this paper here: <https://typeset.io/papers/robust-sensitive-and-automated-phosphopeptide-enrichment-ff7k1s5h0d>

Robust, sensitive and automated phosphopeptide enrichment applied to primary hippocampal neurons

Harm Post^{1#}, Renske Penning^{1#}, Martin A Fitzpatrick¹, Luc B Garrigues¹, Harold D MacGillavry², Casper C Hoogenraad², Albert JR Heck¹, AF Maarten Altelaar^{1,*}

¹*Biomolecular Mass Spectrometry and Proteomics, Bijvoet Center for Biomolecular Research and Utrecht Institute for Pharmaceutical Sciences, Utrecht University, Padualaan 8, 3584 CH Utrecht, The Netherlands and Netherlands Proteomics Centre, Padualaan 8, 3584 CH Utrecht, The Netherlands*

²*Cell Biology, Department of Biology, Faculty of Science, Utrecht University, 3584 CH Utrecht, The Netherlands*

*#Both authors contributed equally to the work, * to whom correspondence should be addressed*

Abstract

Due to the low stoichiometry of protein phosphorylation targeted enrichment prior to LC-MS/MS analysis is still essential. The trend in phosphoproteome analysis is shifting towards increasing numbers of biological replicates per experiment, ideally starting from very low sample amounts, placing new demands on enrichment protocols to make them less labor-intensive, sensitive and less prone to variability. Here, we assessed an automated enrichment protocol using Fe(III)-IMAC cartridges on a AssayMAP Bravo platform to tackle these issues. The automated Fe(III)-IMAC-based enrichment workflow proved to be more effective when compared to a TiO₂-based enrichment using the same platform and a manual Ti(IV)-IMAC-based enrichment workflow. As initial samples we used dilution series of both HeLa and hippocampal neuron lysates, going down to 0.1 µg of starting material. The optimized workflow proved to be sensitive and reproducible, identifying, localizing and quantifying thousands of phosphopeptides from just micrograms of starting material. To further test the automated workflow in genuine biological applications we monitored EGF-induced signaling in primary rat hippocampal neurons, starting with only 75,000 cells prior to phosphopeptide enrichment, revealing among others induced phosphorylation of two glutamate receptors regulating synaptic plasticity.

Introduction

Protein function and dynamics within the cellular environment are in part defined by posttranslational modifications (PTMs). Phosphorylation is a key component of cellular signal transduction and it plays a critical role in many biological processes, where aberrant protein phosphorylation is often correlated with disease (1-6). This makes phosphorylation one of the best-studied PTMs, most commonly achieved using high-resolution mass spectrometry (MS), because of its ability to localize phosphosites to specific amino acids. (7, 8) Unfortunately, as phosphorylation is often of low stoichiometry and covers a high dynamic range, characterization by MS is not straightforward (2, 9, 10).

In the past decade, a multitude of technological developments have substantially advanced large-scale phosphoproteome profiling (11-13). Most methods employ a targeted enrichment of phosphorylated peptides prior to LC-MS/MS analysis, using either ion exchange chromatography (2, 14-16), phospho (motif) specific antibodies (17, 18), metal oxide surfaces (TiO₂) (19, 20) or chelation (21, 22). Recently, a new generation of chelation materials has allowed excellent and robust enrichment of phosphopeptides. These monodisperse microspheres-based immobilized metal ion affinity chromatography (IMAC) resins incorporate flexible linkers that are terminated by phosphonate groups that chelate metal ions. These materials offer superior coordination of phosphorylated peptides in a robust fashion, tolerating the use of harsh solvent conditions. Various metal ions including Ga(II) (22, 23), Ti(IV) (24, 25) and Fe(III) (21) have been used in these IMAC-based phosphopeptide enrichment methods.

Due to the combination of low stoichiometry of phosphopeptides and the resulting need for enrichment, the amount of starting material required for the recovery of a comprehensive phosphoproteome has so far been relatively large, especially when compared to standard proteome

analysis (26). This induces a problem in the analysis of primary cell cultures, laser dissected cells, organoids or tissue samples where available sample quantities are typically low. With increasingly complex experiments (i.e. more time-points, more biological replicates) manually conducted experiments can become very labor intensive. Although we previously already showed that Ti(IV)-IMAC-based enrichment can be qualitatively and quantitatively reproducible (27), the many steps in the protocol make it sensitive to sample variability. To enhance reproducibility in large experimental setups and samples losses, the total sample handling variability should ideally be further minimized. One approach to achieve this is through miniaturization and automation, which allows for processing of multiple samples in parallel, with resulting increased efficiency and reduced variability.

Last year EasyPhos was developed as a first approach to perform phosphoproteomics in an automated workflow (28). While it revealed the potential of automated phosphopeptide enrichment, relatively large amounts of protein input material (1mg) were used. More recently Abelin *et al.* (29) demonstrated that a combination of Fe(III)-IMAC cartridges and an automated platform, the Agilent AssayMap Bravo Platform, enables the identification of over 10,000 unique phosphosites, combining three cell lines treated with 27 compounds (including DMSO). However, also these experiments were conducted by using relatively large amounts of starting material (0.5 mg). Taking the latter Fe(III)-IMAC based automated workflow as starting point we here explored whether this workflow could also be used when starting with up to 1000 times lower sample amounts, and thus also applied to challenging biological samples, such as primary neurons.

Materials and Methods

Cell cultures

HeLa cells were grown in Dulbecco's Modified Eagle Medium (DMEM) supplemented with 10% fetal bovine serum and 10mM glutamine (all from Lonza, Braine-l'Alleud, Belgium). Six hours before harvesting, the medium was replaced by fresh medium. Cells were harvested and the cell pellets were immediately washed two times with phosphate-buffered saline buffer (PBS) and stored at -80°C till further usage.

Dissociated hippocampal neuron cultures were prepared from embryonic day 18 rats of either sex. Cells were plated at a density of 75,000 per well and treated as described before (30). At day 14-15 cells were stimulated with either vehicle or 10 ng/ml Epidermal Growth Factor (EGF, Sigma-Aldrich) for 20 minutes. Cells were harvested and washed with PBS and stored at -80°C till further usage.

Protein lysis and digestion

Cells were lysed in lysis buffer (1% sodiumdeoxycholate (SDC), 10mM tris(2-carboxyethyl)phosphinehydrochloride (TCEP), 40mM chloroacetamide (CAA) and 100 mM TRIS, pH 8.0 supplemented with phosphatase inhibitor (PhosSTOP, Roche) and protease inhibitor (cOmplete mini EDTA-free, Roche). Cells were heated for 5 min at 95°C, sonicated with the Bioruptor Plus (Diagenode) for 15 cycles of 30 sec and diluted 1:10 with 50 mM ammoniumbicarbonate, pH 8.0. Proteins were digested overnight at 37°C with trypsin (Sigma-Aldrich) with an enzyme/substrate ratio of 1:50 and Lysyl Endopeptidase (Lys-C, Wako) with an enzyme/substrate ratio of 1:75. SDC was precipitated with 2% formic acid (FA) and samples were desalted using Sep-Pak C18 cartridges (Waters) and eluted with 80% acetonitrile (ACN)/0.1% trifluoroacetic acid (TFA) and directly subjected to phosphopeptide enrichment or dried down and stored in -80°C till further use.

Phosphorylated peptide enrichment

Manual Ti(IV)-IMAC-based workflow

Phosphopeptide enrichment was performed as described as before (25). Briefly, the Ti(IV)-beads were packed into a Geloader microtip column and washed with methanol and loading buffer (80% (ACN)/ 6% TFA. Samples were dissolved in loading buffer and loaded onto the beads. Columns were washed with 50% ACN/0.5% TFA in 200 mM NaCl and 50% ACN/0.1% TFA and phosphopeptides were eluted with 10% ammonia and 80% ACN/2%FA directly in 10% FA. Samples were dried down and stored in -80°C till LC-MS/MS analysis.

Automated TiO₂ and Fe(III)-IMAC-based workflows

Phosphorylated peptides were enriched using either TiO₂ or Fe(III)-NTA cartridges (Agilent technologies) in an automated fashion using the AssayMAP Bravo Platform (Agilent technologies). TiO₂ columns were primed with 5% ammonia / 15% ACN and equilibrated with loading buffer (50% ACN/2% TFA). Samples were dissolved in loading buffer and loaded onto the column. The cartridges were washed with loading buffer and the phosphorylated peptides were eluted with 5% ammonia directly into 10% formic acid and dried down. Fe(III)-NTA cartridges were primed with 0.1% TFA in ACN and equilibrated with loading buffer (80% ACN/0.1% TFA). Samples were dissolved in loading buffer and loaded onto the cartridge. The columns were washed with loading buffer and the phosphorylated peptides were eluted with 1% ammonia directly into 10% formic acid. Samples were dried down and stored in -80° C till subjected to LC-MS.

Mass spectrometry: RP-nanoLC-MS/MS

The data were acquired using an Agilent 1290 system coupled to an Orbitrap Q Exactive Plus mass spectrometer (Thermo Scientific). Peptides were first trapped (Dr Maisch Reprisil C18, 3 µm, 2 cm x 100

μm) before being separated on an analytical column (Agilent Poroshell EC-C18, 2.7 μm , 50 cm x 75 μm). Trapping was performed for 10 min in solvent A (0.1 M acetic acid in water) and the gradient was as follows; 4 - 8% solvent B (0.1 M acetic acid in 80% acetonitrile) in 2 min, 8 - 24% in 71 min, 24 - 35% in 16 min, 35 - 60% in 7 min, 60 - 100% in 2 min and finally 100 % for 1 min. Flow was passively split to 300 nl min^{-1} . The mass spectrometer was operated in data-dependent mode. Full scan MS spectra from m/z 375 – 1600 were acquired at a resolution of 35,000 at m/z 400 after accumulation to a target value of $3\text{E}6$. Up to ten most intense precursor ions were selected for fragmentation. HCD fragmentation was performed at normalised collision energy of 25% after the accumulation to a target value of $5\text{E}4$. MS/MS was acquired at a resolution of 17,500.

Data analysis

Raw files were processed using MaxQuant (version 1.5.3.30). The database search was performed against the human Swissprot database (version 25th of June 2015) or the Rattus Norvegicus Ensemble database (version 12th of March 2016) using Andromeda as search engine. Cysteine carbamidomethylation was set as a fixed modification and methionine oxidation, protein N-term acetylation and phosphorylation of serine, threonine and tyrosine were set as variable modifications. Trypsin was specified as enzyme and up to two miss cleavages were allowed. Filtering was done at 1% false discovery rate (FDR) at the protein and peptide level. Label free quantification (LFQ) was performed and 'match between runs' was enabled.

Quantified data were processed and analysed using a custom Python package (PaDuA) to remove potential contaminants and reverse peptides, filtered for localization probability > 0.75, \log_2 transformed and normalized to column median as per standard methods. Statistical analysis, including Principal Component Analysis (PCA), correlation and clustering were performed on the processed data.

Results and Discussion

Our aim was to explore the AssayMAP Bravo Platform automated phosphopeptide enrichment workflow for high throughput phosphoproteome analysis using small amounts of starting material. We first evaluated the performance of the manufacturer supplied TiO_2 and Fe(III)-IMAC cartridges on the Agilent AssayMAP Bravo Platform against our own established manual Ti(IV)-IMAC-based phosphopeptide workflow described previously (25, 27) (Figure 1A). After lysis of HeLa cells using the SDC protocol, protein extracts were digested using subsequently Lys-C and trypsin and 200 μg of the resulting peptides were subjected to either TiO_2 or Fe(III)-IMAC based automated phosphopeptide enrichment, or manual enrichment using the Ti(IV)-IMAC-based workflow. As shown in Figure 2A, the Fe(III)-IMAC and Ti(IV)-IMAC-based workflows outperformed the TiO_2 based workflow, with 22-34% more uniquely identified phosphosites in four consecutive enrichments. On average 7,672 unique phosphosites were identified in a single enrichment using Ti(IV)-IMAC, 8,110 phosphosites in Fe(III)-IMAC and 5,980 phosphosites in the TiO_2 based enrichments. The relative low performance of the TiO_2 was unexpected, as we recently demonstrated equal performance of TiO_2 and Ti(IV)-IMAC in a manual approach (9). The relative low performance of the TiO_2 automated workflow on the AssayMAP Bravo Platform can most likely be explained by the use of non-ideal buffer conditions compared to our manual approach. The high concentration of TFA in the buffers used for the manual approach is not compatible with the cartridges in the Bravo Platform. The enrichments using Fe(III)-IMAC and Ti(IV)-IMAC were highly specific (>90%) (Figure 2B), while TiO_2 displayed an enrichment specificity of just 50%, much lower than the 85-95% we demonstrated earlier in our manual TiO_2 workflow. For quantitative analysis we filtered out the (Class I; ≥ 0.75) phosphosites being detected in at least 2 replicates, cumulatively resulting in 6,408 phosphosites for Ti(IV)-IMAC, 6,973 for Fe(III)-IMAC and 4,756 for TiO_2 (see Supplementary Data T1). This stringent filtering was used for all below reported analyses. Previously we showed that the manual approach using Ti(IV)-IMAC is quite reproducible and can be used for quantitative phosphoproteome

analysis using label-free quantification based on peptide ion intensities. Here, we evaluated whether the automated workflows (using either Fe(III)-IMAC or TiO₂) can also be used for quantitative phosphoproteome profiling, and whether this quantitation is possible enrichment workflow dependent. We thus compared, focusing on the unique phosphopeptides detected in all enrichments, the phosphopeptide ion intensities. Although, the overall correlation between experiments is very good, the data displayed in Figure 2E, reveals that the correlation is best when a single enrichment is used, and weaker when we for instance compare data from a TiO₂ enrichment with a Fe(III)-IMAC-based enrichment. This behaviour was further extracted from a principal component analysis (Figure 2C) that revealed that the replicate enrichments for each workflow cluster together indicating strong reproducibility, with Fe(III)-IMAC and Ti(IV)-IMAC being most similar. The overlap in enriched phosphopeptides between the different methods was high (Figure 2D) with 91% overlap between Ti(IV)-IMAC and Fe(III)-IMAC and 84% between Fe(III)-IMAC and TiO₂ and 76% found for all three methods in at least 1 out of 4 replicates per method.

Based on these results, we were especially satisfied with the performance of the Fe(III)-IMAC-based automated platform in comparison with the manual Ti(IV)-IMAC approach and decided to further characterise and validate the performance of this approach. As shown above the Fe(III)-IMAC cartridges showed excellent performance using 200 µg of HeLa digest. However, in many biological experiments the amount of material can be much smaller. Thus next we assessed the performance of the Fe(III)-IMAC cartridges using variable amounts of HeLa digest (0.1 – 500 µg). As expected and displayed in Figure 3A, the number of identified phosphopeptides was lower when starting with very low amounts of input material. Remarkably though, starting with only 100 ng of HeLa digest we were still able to identify 215 unique phosphopeptides, with 1 µg this increased to 1443 unique phosphopeptides, and with 10 µg of HeLa digest 4541 unique phosphopeptides were identified. Cumulatively, the replicate enrichments of 100 ng resulted in 319 unique phosphopeptides and 415 class I phosphosites in at least 2 replicates, 1 µg

in 1903 unique phosphopeptides and 1694 phosphosites, and 10 μg in 5726 unique phosphopeptides and 4324 phosphosites. Using 200 μg of input material resulted in an optimal performance of the Fe(III)-IMAC cartridges with over 8269 unique phosphopeptides being identified and 5697 class I phosphosites quantified in at least 2 replicates using a single LC MS/MS analysis per enrichment. The qualitative reproducibility was high for all enrichment amounts with an overlap of >65% between consecutive enrichments (see Figure S1). The reproducibility decreased once less than 1 μg of HeLa digest was used. Next to the qualitative, the quantitative reproducibility was also very high between consecutive HeLa digest enrichments when using the same amount of starting material, with an average correlation of $R = 0.87$, comparable to the correlation observed in the technical replicate LC-MS runs (27, 28). Interestingly, the Pearson correlation remained high when, after normalisation, the different amounts of starting material were compared (Figure S1A). Two relative outliers were observed, namely the two extreme cases in the amount of starting material, 0.1 μg and 500 μg in the HeLa digest. It may not be surprising that the correlation decreased most for the 0.1 μg samples, where the signal to noise in the LC MS/MS is poorest. The lower correlation observed when starting with 500 μg of HeLa digest can most likely be explained by an overloading of the cartridge, although identification rates were still high. Furthermore Figure 3A shows that the vast majority of phosphopeptides identified in the 200 μg HeLa sample could already be identified, in the analysis using much lower sample amounts. Evidently in the case of lab-cultured HeLa cells the sample quantity is not likely a limiting factor. We next analysed the phosphoproteome of rat primary hippocampal neurons. These primary neuronal cells are typically plated in 6-well format with a density of 75,000 cells per well, leading to approximately 50 μg of proteinaceous material per sample. Due to the specialized function of neuronal cells, we hypothesized a larger dynamic range in protein expression and relatively lower phosphorylation levels compared to the HeLa cell digests. We tested the Fe(III)-IMAC-based automated enrichment method on these primary neurons in triplicate using again a dilution series ranging from 1 to 25 μg , prepared from a pooled

neuronal protein extract. With only 25 μg of input material an average of 3,615 phosphopeptides could be identified and by starting with 1 μg of material we could still identify 1,963 unique phosphopeptides (Figure 3B). Cumulatively, 2,926 class I phosphosites were quantified in at least 2 replicates for 25 μg starting material and 1,098 for 1 μg . The overlap between the different starting amounts was high with 98% of the phosphopeptides in the 25 μg sample identified in the samples using lower starting amounts. When comparing equal amounts of HeLa cells and neurons, we found a lower number of phosphorylated peptides in the neuron samples, although nicely in the neuron samples the correlations at the label-free quantitative level were high (Figure S1B).

To inspect the detectable dynamic range of the enrichment method in combination with the LC-MS/MS analysis, we plotted the normalized MS signal intensities observed for the samples derived from different quantities of starting material, for both the HeLa and neuron samples, as shown in Figure S2A-S2D. For both sample types the detectable dynamic range was substantially smaller for the lower sample amounts, suggesting that with less starting material only the more high abundant phosphopeptides are being enriched and detected. As shown in Figure S2E and S2F indeed an overrepresentation of phosphopeptides with a high ion intensities is observed. Together, these two datasets demonstrate that even with low quantities of material (down to 1 μg) one can already not only identify but also quantify thousands of phosphorylated peptides in a reliable manner.

To further test the performance of the automated workflow in quantitative phosphoproteome profiling, we investigated the phosphorylation dynamics in primary rat hippocampal neurons upon stimulation with EGF (Figure 4). The EGF receptor is highly expressed in hippocampal neurons (31). We stimulated hippocampal neurons with 10 ng/ml EGF for 20 minutes and quantitatively monitored changes in the phosphorylation profiles, compared to neurons treated only with the vehicle as control. A six well plate format was used with only one well per condition, both conditions in triplicate, resulting in a maximum of 50 μg of protein input material for the Fe(III)-IMAC phosphopeptide enrichment. From these

phosphopeptide enrichments we subjected 40% to single run LC-MS/MS, resulting in the identification of 6,095 unique phosphopeptides from which 4,611 class I phosphosites could be quantified in at least 2 replicates. We assessed the quality of this experiment by plotting Pearson correlations of the EGF and control samples (Figure 4a), showing high quantitative reproducibility, comparable to the first experiment with the non-stimulated neuron samples. Notably, the Pearson correlations of the EGF treated neurons increased compared to the untreated samples, respectively >0.98 and >0.83, likely the consequence of synchronization of phosphorylation events in the stimulated neurons in response to EGF. A two-sample *t*-test revealed 789 significantly regulated phosphosites at a false discovery rate (FDR) of 5% (Figure 4B). EGF is known to influence the phosphorylation status of proteins belonging to the MAPK pathway, of which multiple members could be quantified with our method. Indeed many of these proteins were found to be strongly regulated following EGF stimulation (Figure 4C). Moreover, it has been reported that EGF stimulation can influence the NMDA receptor mediated response in hippocampal neurons, altering the calcium influx and potentially plasticity and long term potentiation (LTP) of synapses (31, 32). Therefore, we also examined our data for phosphorylation dynamics related to LTP. Strikingly, the enrichment method applied here was sensitive enough to detect changes in receptor phosphorylation status even when starting the experiments with these low sample amounts. For instance, the known phosphosite S886 for the NMDAR receptor Grin2B of the glutamate-gated ion channel (33, 34) was significantly elevated after EGF treatment, while phosphorylation of two sites on the mGluR5 receptor, S860 and S839 (see Figure 5A/B), were significantly down-regulated. It is known that S839 phosphorylation is required for the unique calcium oscillations triggered by mGluR5 activation (35). Furthermore, we observed decreased phosphorylation of S853 on the glutamate receptor mGluR1 α . When the sequences of mGluR5 and mGluR1 α were aligned both S839 and S853 show alike motifs (35) (Figure 5C) and therefore similar behaviour of these phosphosites could be expected. It has been shown previously that regulation of mGluR5 by an agonist influences the phosphorylation status of

the EGF receptor in rat cortical astrocytes and striatal neurons, although the link was so far mainly shown via tyrosine kinase signalling (36, 37). Here we observe that the reverse behaviour is also occurring and that EGF receptor stimulation in turn influences the phosphorylation status of the mGluR5 receptor (Figure 4C). Together, these results indicate that a more detailed analysis of the here observed receptor behaviour, involved in among others LTP, would be interesting for future research.

Conclusion

So far is mass spectrometry based phosphoproteomics a good coverage of the phosphoproteome related very much on total amount of sample available. Moreover, many current workflows in phosphoproteomics are seriously hampered by a lack of reproducibility. As the tendency in phosphoproteomics is shifting towards the analysis of samples increasingly more related to human patients, such as patient primary cells, organoids and cells FACS sorted or micro-dissected from tissue, more sensitive and more robust methods are needed, enabling high reproducibility in at least technical replicates. Here, we assessed an automated and miniaturize enrichment protocol using Fe(III)-IMAC cartridges on a AssayMAP Bravo platform and found it to provide an efficient, sensitive and reproducible approach for phosphoproteomic analysis. We demonstrate reproducible enrichment of thousands of phosphorylated peptides in a qualitative and quantitative manner from a limited amount of starting material, even down to the sub-microgram level. The potential of this workflow was demonstrated by our quantitative analysis of the phosphorylation dynamics in EGF stimulated rat hippocampal neurons, using material from single wells containing approximately 75,000 neuron cells, revealing the regulation of functional phosphosites on many proteins in the activated MAP kinase pathway and even several membrane incorporated glutamate receptors.

Acknowledgements

The authors would like to thank Wei Wu for providing the HeLa samples. This work was partly supported by the *Proteins@Work*, a program of the Netherlands Proteomics Centre financed by the Netherlands Organisation for Scientific Research (NWO) as part of the National Roadmap Large-scale Research Facilities of the Netherlands (project number 184.032.201). This project received also funding from the European Union's Horizon 2020 research and innovation programme (grant agreement MSMed No. 686547) and 7th framework programme (grant agreement Manifold No. 317371)".

References

1. Pagel O, Loroach S, Sickmann A, Zahedi RP. Current strategies and findings in clinically relevant post-translational modification-specific proteomics. *Expert Rev Proteomics*. 2015 Jun;12(3):235-53.
2. Zhou H, Di Palma S, Preisinger C, Peng M, Polat AN, Heck AJ, et al. Toward a comprehensive characterization of a human cancer cell phosphoproteome. *J Proteome Res*. 2013 Jan 4;12(1):260-71.
3. Hunter T. Protein kinases and phosphatases: the yin and yang of protein phosphorylation and signaling. *Cell*. 1995 Jan 27;80(2):225-36.
4. Ubersax JA, Ferrell JE, Jr. Mechanisms of specificity in protein phosphorylation. *Nat Rev Mol Cell Biol*. 2007 Jul;8(7):530-41.
5. Hunter T. Tyrosine phosphorylation: thirty years and counting. *Curr Opin Cell Biol*. 2009 Apr;21(2):140-6.
6. Pawson T, Scott JD. Protein phosphorylation in signaling--50 years and counting. *Trends Biochem Sci*. 2005 Jun;30(6):286-90.
7. Altelaar AF, Munoz J, Heck AJ. Next-generation proteomics: towards an integrative view of proteome dynamics. *Nat Rev Genet*. 2013 Jan;14(1):35-48.
8. Riley NM, Coon JJ. Phosphoproteomics in the Age of Rapid and Deep Proteome Profiling. *Anal Chem*. 2016 Jan 5;88(1):74-94.
9. Matheron L, van den Toorn H, Heck AJ, Mohammed S. Characterization of biases in phosphopeptide enrichment by Ti(4+)-immobilized metal affinity chromatography and TiO₂ using a massive synthetic library and human cell digests. *Anal Chem*. 2014 Aug 19;86(16):8312-20.
10. Mann M, Ong SE, Gronborg M, Steen H, Jensen ON, Pandey A. Analysis of protein phosphorylation using mass spectrometry: deciphering the phosphoproteome. *Trends Biotechnol*. 2002 Jun;20(6):261-8.

11. Giansanti P, Aye TT, van den Toorn H, Peng M, van Breukelen B, Heck AJ. An Augmented Multiple-Protease-Based Human Phosphopeptide Atlas. *Cell Rep.* 2015 Jun 23;11(11):1834-43.
12. Sharma K, D'Souza RC, Tyanova S, Schaab C, Wisniewski JR, Cox J, et al. Ultradeep human phosphoproteome reveals a distinct regulatory nature of Tyr and Ser/Thr-based signaling. *Cell Rep.* 2014 Sep 11;8(5):1583-94.
13. Batth TS, Francavilla C, Olsen JV. Off-line high-pH reversed-phase fractionation for in-depth phosphoproteomics. *J Proteome Res.* 2014 Dec 5;13(12):6176-86.
14. Gauci S, Helbig AO, Slijper M, Krijgsveld J, Heck AJ, Mohammed S. Lys-N and trypsin cover complementary parts of the phosphoproteome in a refined SCX-based approach. *Anal Chem.* 2009 Jun 1;81(11):4493-501.
15. Beausoleil SA, Jedrychowski M, Schwartz D, Elias JE, Villen J, Li J, et al. Large-scale characterization of HeLa cell nuclear phosphoproteins. *Proc Natl Acad Sci U S A.* 2004 Aug 17;101(33):12130-5.
16. Nuhse TS, Stensballe A, Jensen ON, Peck SC. Large-scale analysis of in vivo phosphorylated membrane proteins by immobilized metal ion affinity chromatography and mass spectrometry. *Mol Cell Proteomics.* 2003 Nov;2(11):1234-43.
17. Giansanti P, Stokes MP, Silva JC, Scholten A, Heck AJ. Interrogating cAMP-dependent kinase signaling in Jurkat T cells via a protein kinase A targeted immune-precipitation phosphoproteomics approach. *Mol Cell Proteomics.* 2013 Nov;12(11):3350-9.
18. Pandey A, Podtelejnikov AV, Blagoev B, Bustelo XR, Mann M, Lodish HF. Analysis of receptor signaling pathways by mass spectrometry: identification of vav-2 as a substrate of the epidermal and platelet-derived growth factor receptors. *Proc Natl Acad Sci U S A.* 2000 Jan 4;97(1):179-84.
19. Larsen MR, Thingholm TE, Jensen ON, Roepstorff P, Jorgensen TJ. Highly selective enrichment of phosphorylated peptides from peptide mixtures using titanium dioxide microcolumns. *Mol Cell Proteomics.* 2005 Jul;4(7):873-86.
20. Pinkse MW, Uitto PM, Hilhorst MJ, Ooms B, Heck AJ. Selective isolation at the femtomole level of phosphopeptides from proteolytic digests using 2D-NanoLC-ESI-MS/MS and titanium oxide precolumns. *Anal Chem.* 2004 Jul 15;76(14):3935-43.
21. Andersson L, Porath J. Isolation of phosphoproteins by immobilized metal (Fe³⁺) affinity chromatography. *Anal Biochem.* 1986 Apr;154(1):250-4.
22. Posewitz MC, Tempst P. Immobilized gallium(III) affinity chromatography of phosphopeptides. *Anal Chem.* 1999 Jul 15;71(14):2883-92.
23. Aryal UK, Olson DJ, Ross AR. Optimization of immobilized gallium (III) ion affinity chromatography for selective binding and recovery of phosphopeptides from protein digests. *J Biomol Tech.* 2008 Dec;19(5):296-310.

24. Zhou H, Ye M, Dong J, Han G, Jiang X, Wu R, et al. Specific phosphopeptide enrichment with immobilized titanium ion affinity chromatography adsorbent for phosphoproteome analysis. *J Proteome Res.* 2008 Sep;7(9):3957-67.
25. Zhou H, Ye M, Dong J, Corradini E, Cristobal A, Heck AJ, et al. Robust phosphoproteome enrichment using monodisperse microsphere-based immobilized titanium (IV) ion affinity chromatography. *Nat Protoc.* 2013 Mar;8(3):461-80.
26. Zhong J, Molina H, Pandey A. Phosphoproteomics. *Curr Protoc Protein Sci.* 2007 Nov;Chapter 24:Unit 24.4.
27. de Graaf EL, Giansanti P, Altelaar AF, Heck AJ. Single-step enrichment by Ti⁴⁺-IMAC and label-free quantitation enables in-depth monitoring of phosphorylation dynamics with high reproducibility and temporal resolution. *Mol Cell Proteomics.* 2014 Sep;13(9):2426-34.
28. Humphrey SJ, Azimifar SB, Mann M. High-throughput phosphoproteomics reveals in vivo insulin signaling dynamics. *Nat Biotechnol.* 2015 Sep;33(9):990-5.
29. Abelin JG, Patel J, Lu X, Feeney CM, Fagbami L, Creech AL, et al. Reduced-representation phosphosignatures measured by quantitative targeted MS capture cellular states and enable large-scale comparison of drug-induced phenotypes. *Mol Cell Proteomics.* 2016 Feb 24.
30. Frost NA, Shroff H, Kong H, Betzig E, Blanpied TA. Single-molecule discrimination of discrete perisynaptic and distributed sites of actin filament assembly within dendritic spines. *Neuron.* 2010 Jul 15;67(1):86-99.
31. Tang Y, Ye M, Du Y, Qiu X, Lv X, Yang W, et al. EGFR signaling upregulates surface expression of the GluN2B-containing NMDA receptor and contributes to long-term potentiation in the hippocampus. *Neuroscience.* 2015 Sep 24;304:109-21.
32. Abe K, Saito H. Epidermal growth factor selectively enhances NMDA receptor-mediated increase of intracellular Ca²⁺ concentration in rat hippocampal neurons. *Brain Res.* 1992 Jul 31;587(1):102-8.
33. Lundby A, Secher A, Lage K, Nordsborg NB, Dmytriyev A, Lundby C, et al. Quantitative maps of protein phosphorylation sites across 14 different rat organs and tissues. *Nat Commun.* 2012 Jun 6;3:876.
34. Ghafari M, Hoyer H, Keihan Falsafi S, Russo-Schlaff N, Pollak A, Lubec G. Mass spectrometrical identification of hippocampal NMDA receptor subunits NR1, NR2A-D and five novel phosphorylation sites on NR2A and NR2B. *J Proteome Res.* 2012 Mar 2;11(3):1891-6.
35. Kim CH, Braud S, Isaac JT, Roche KW. Protein kinase C phosphorylation of the metabotropic glutamate receptor mGluR5 on Serine 839 regulates Ca²⁺ oscillations. *J Biol Chem.* 2005 Jul 8;280(27):25409-15.
36. Peavy RD, Chang MS, Sanders-Bush E, Conn PJ. Metabotropic glutamate receptor 5-induced phosphorylation of extracellular signal-regulated kinase in astrocytes depends on transactivation of the epidermal growth factor receptor. *J Neurosci.* 2001 Dec 15;21(24):9619-28.

37. Yang L, Mao L, Chen H, Catavsan M, Kozinn J, Arora A, et al. A signaling mechanism from G alpha q-protein-coupled metabotropic glutamate receptors to gene expression: role of the c-Jun N-terminal kinase pathway. *J Neurosci*. 2006 Jan 18;26(3):971-80.

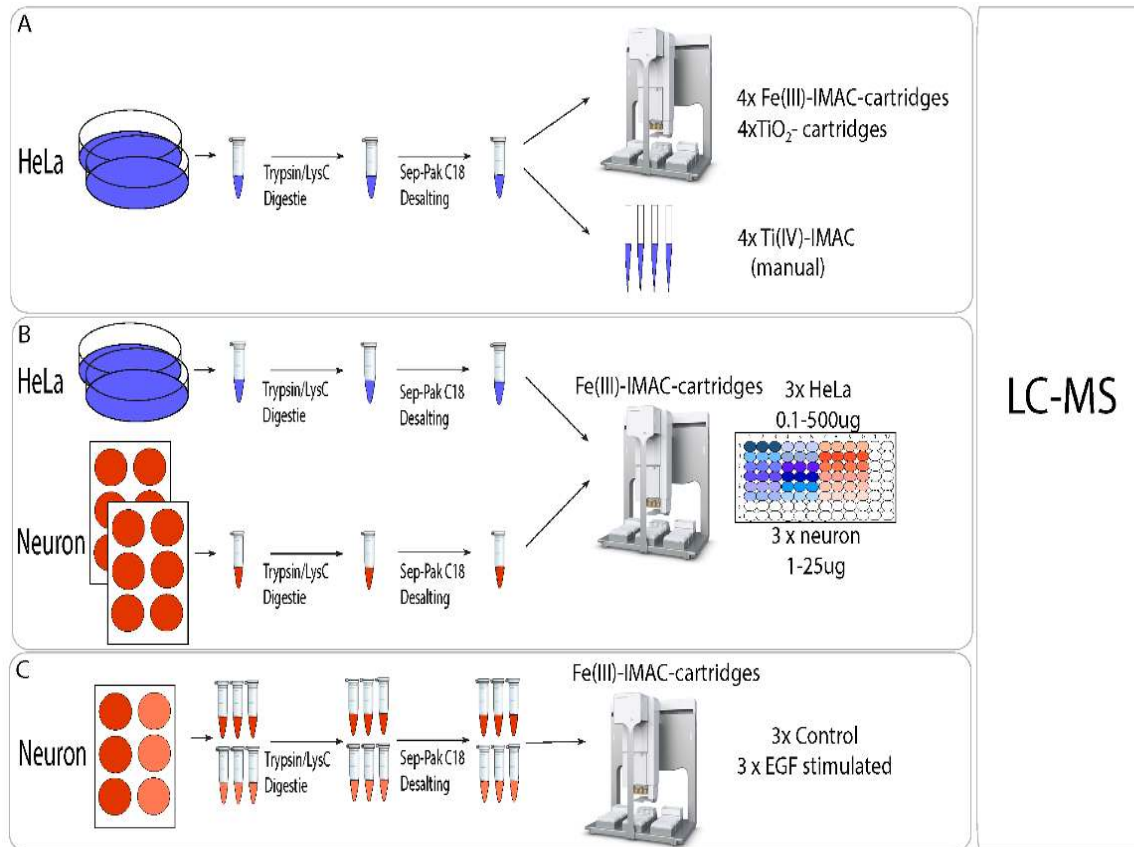


Figure 1. Overview of used workflows for sensitive phosphoproteome analysis. *A.* Assessment of performance of three enrichment strategies; namely manually using Ti(IV)-IMAC loaded tips, or automated using the Bravo Assay Map with either Fe(III)-IMAC or TiO₂ loaded cartridges. *B.* Phosphoproteome analysis, using the automated Fe(III)-IMAC based workflow, of varying amounts of a HeLa digest (0.1 µg – 500 µg) and Rat hippocampal neuron digests (1 – 25 µg). *C.* Phosphoproteome analysis, using the automated Fe(III)-IMAC based workflow, of Rat hippocampal neurons digests stimulated with EGF or vehicle for 20 minutes. In all these workflows the samples resulting from the phosphopeptide enrichment were analyzed by using a single run LC-MS/MS using a 100 min gradient on a Q-Exactive plus.

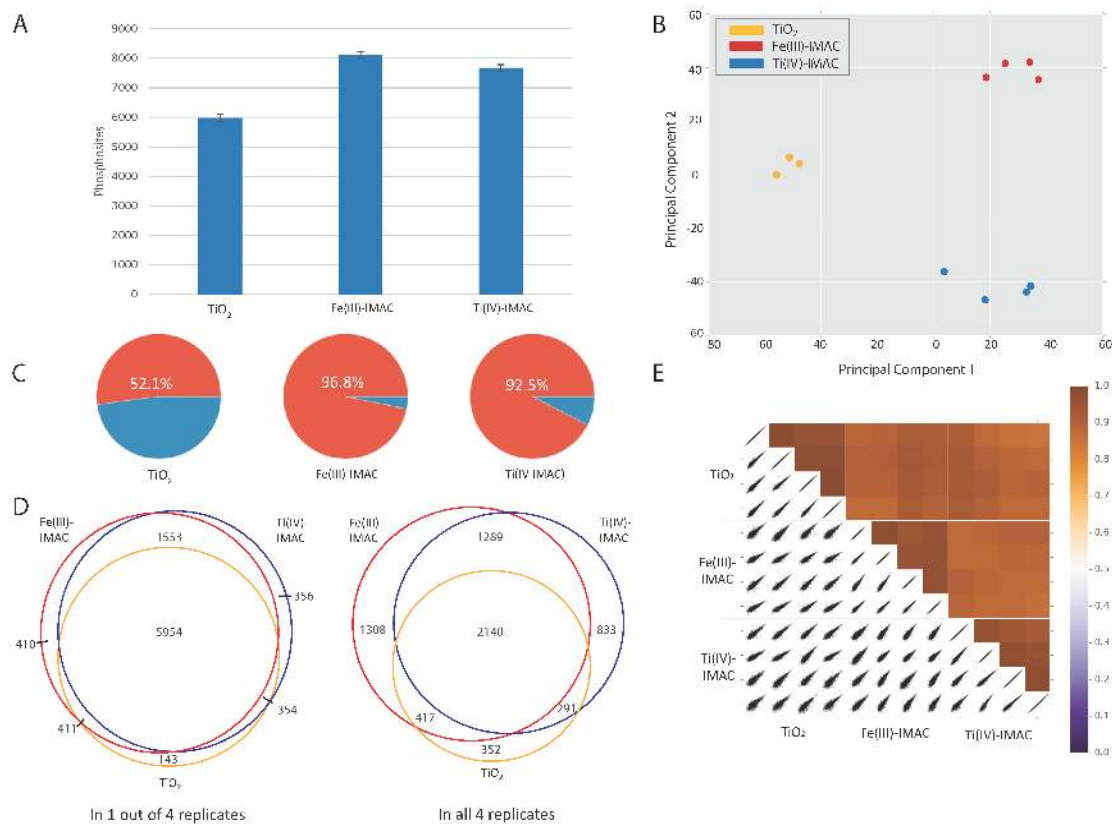


Figure 2. Assessment of performance and characteristics of phosphopeptide enrichment strategies. Three workflows were comparatively assessed, namely a more manual approach using Ti(IV)-IMAC loaded tips, or automated using the Bravo Assay Map with either Fe(III)-IMAC or TiO₂ loaded cartridges, using X mg of Hela digest as input. **A.** Average number of identified phosphosites in a single LC-MS/MS run performed in quadruplicate for the 3 different enrichment protocols. The TiO₂ loaded cartridges systematically underperform (for reasons highlighted in the text), while the automated Fe(III)-IMAC approach performs at least as well as the more labor intensive manual workflow using Ti(IV)-IMAC loaded tips. **B.** Different phosphopeptide enrichment workflows lead to distinctive phosphoproteomes. PCA analysis of the three different used enrichment methods, reveal strong clustering of replicate enrichments using the same workflow that can be distinguished from measurements by alternative workflows **C.** Ratio of identified phosphopeptides *versus* non-phosphorylated peptides for the here applied enrichment workflows, revealing a very good phosphopeptide enrichment efficiency for Ti(IV)-IMAC and Fe(III)-IMAC. The lower efficiency of around 50% for TiO₂ is attributed to the incompatibility of this material with the buffers used in the automated workflow. **D.** Venn diagrams displaying the overlap between the 3 phosphopeptide enrichment methods in identified phosphosites observed in 1 out of 4 replicates and in all 4 replicates, showing a good overlap in identifications between the different methods. **E.** Comparison of label free quantification of phosphopeptides within one enrichment workflow and in between workflows. The heatmap shows the Pearson correlations for the different replicates. Overall the different phosphopeptide enrichment experiments reveal a good correlation, with the highest values observed for data gathered within one single workflow.

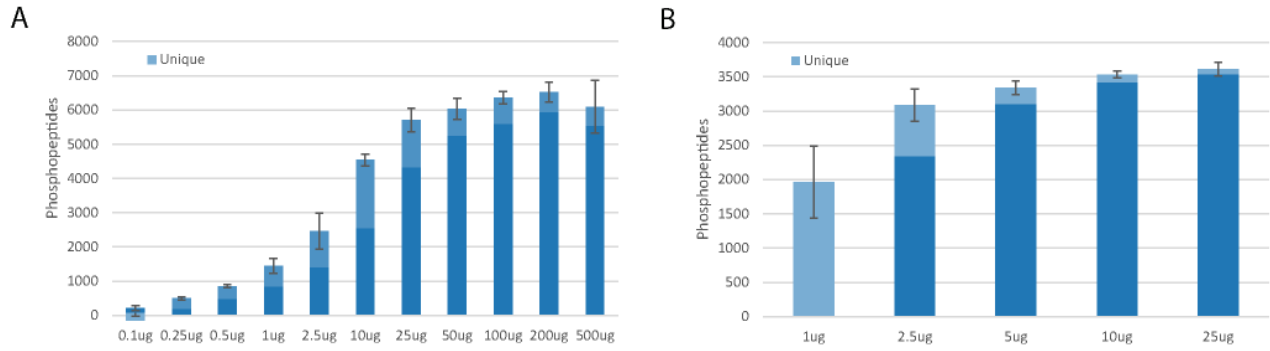


Figure 3. Sensitivity in automated phosphoproteome analysis. Number of phosphopeptides identified, using the automated Fe(III)-IMAC workflow, from various amounts of starting material of A) HeLa digests and B) primary hippocampal neuron digests. The data shows an increasing number of identifications with higher amount of starting material up to 200 μ g for the HeLa digest. Shaded regions indicate the percentage of phosphopeptides also identified at lower concentrations.

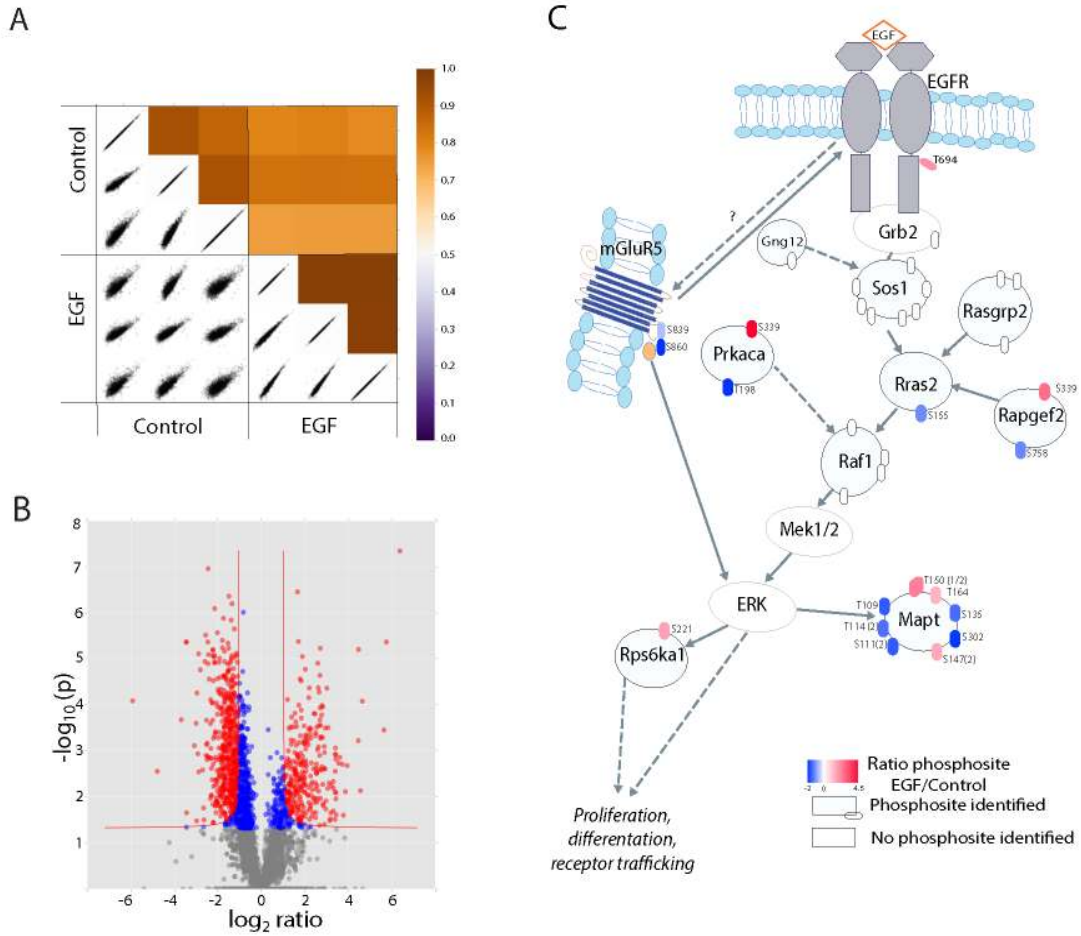


Figure 4. Label-free phosphoproteome analysis of Rat hippocampal neurons stimulated with EGF. *A.* Heatmap of Pearson correlations for the different replicates in the EGF stimulated and control samples showing high quantitative reproducibility between all measurements. *B.* Volcanoplot displaying the differential phosphorylation observed for control *versus* EGF stimulated hippocampal neurons with in red the significantly regulated phosphosites using an FDR of 5%. *C.* Observed regulation of the MAPK pathway in EGF stimulated cells. The sites are colored according to their ratio between the EGF stimulated and control neurons. Two phosphosites of the mGluR5 receptor are clearly regulated, hinting at communication between EGFR and mGluR5.

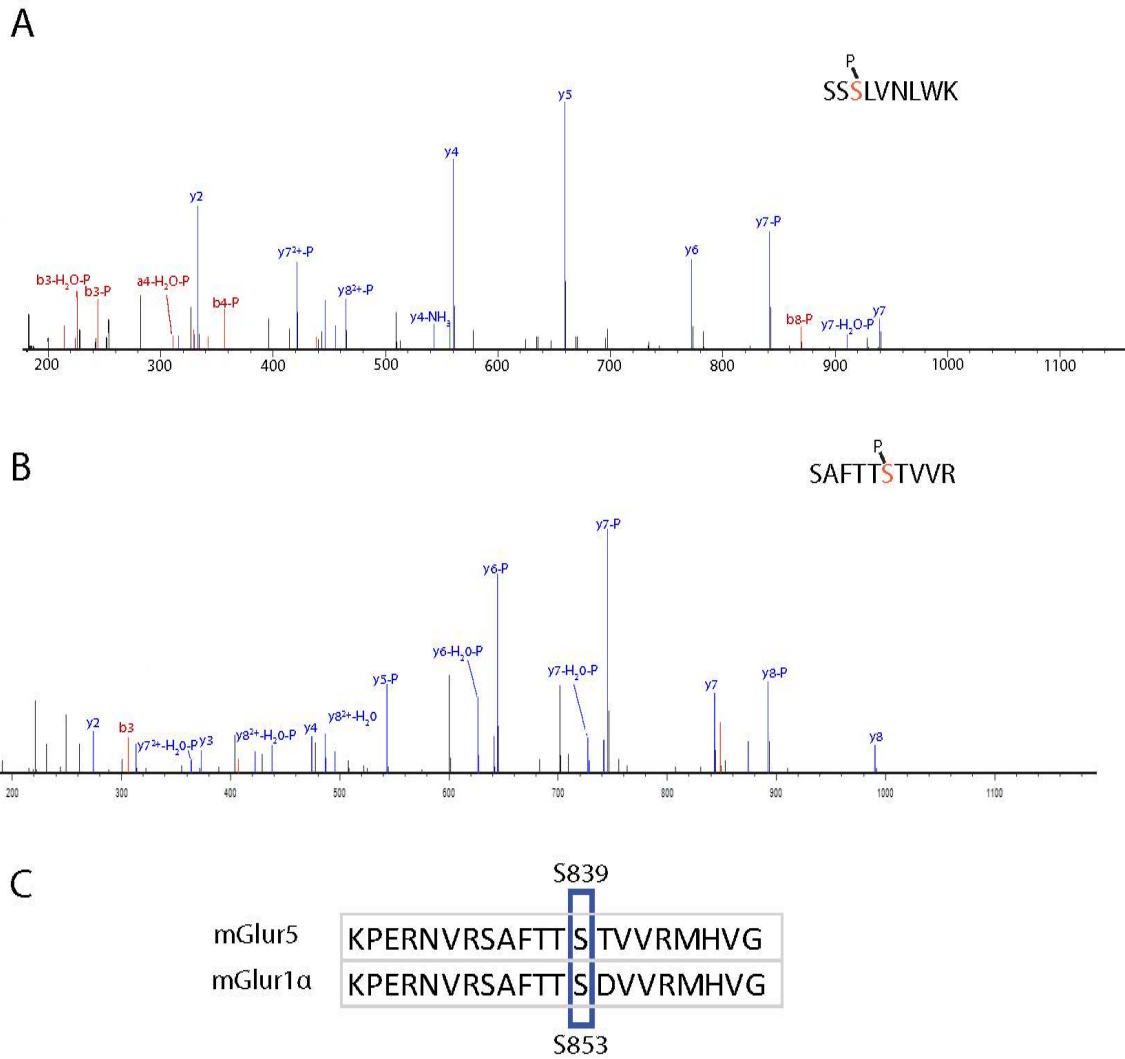


Figure 5. The rat neuron mGlu5 and MGlur1α receptors become phosphorylated upon EGF stimulation. A. Representative HCD spectra of the mGlu5 peptide phosphorylated at S860. B. Representative HCD spectra of the mGlu5 peptide phosphorylated at S839. C. Sequence alignment of the mGlu5 and MGlur1α receptor. The sequences of both receptors around the S839 and S853 phosphosites are very much alike and a similar trend in phosphorylation was observed upon stimulation with EGF.

Supplementary figures:

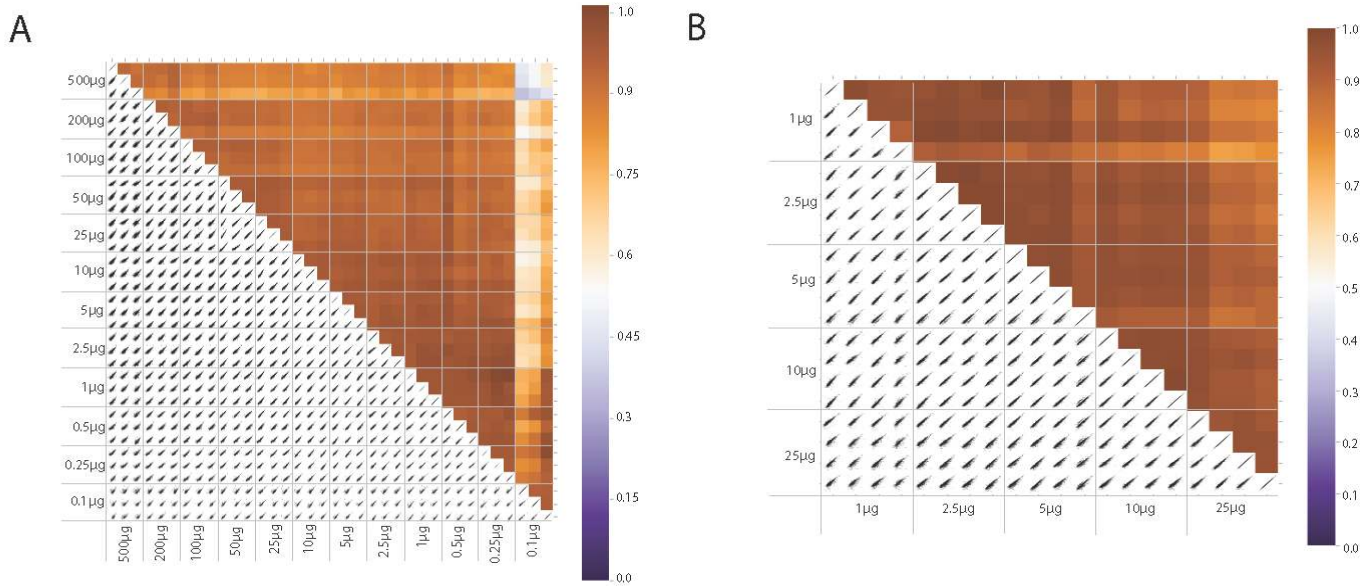


Figure S1. Label free quantitative phosphoproteome analysis of HeLa/neuron digests, using variable amounts of starting material. Pearson correlation plots of Fe(III)-IMAC phosphopeptide enrichment with different amounts of protein starting material from HeLa and rat hippocampal neurons *A*. Pearson correlation plot of the different replicates and different starting amounts for HeLa samples. High quantitative reproducibility between phosphosite intensities within consecutive enrichments per sample amount and between the different starting amounts is observed. *B*. Pearson correlation plot of the different replicates and different starting amounts for the rat hippocampal neuron samples with high quantitative reproducibility between consecutive enrichments for a single amount and between different amounts of material.

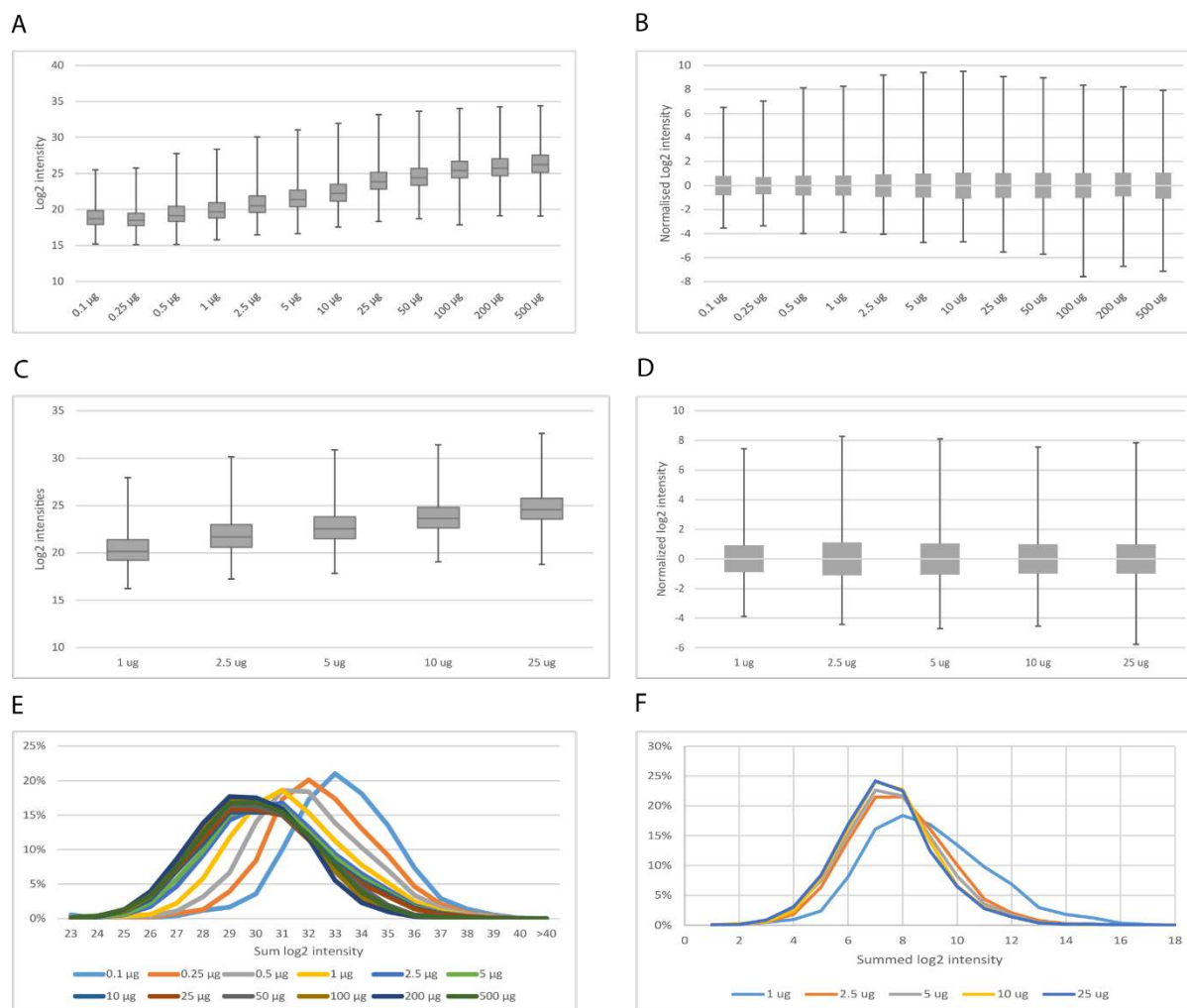


Figure S2. Dynamic range in the phosphoproteome can be extended by using more starting material. Intensity distributions of phosphopeptides enriched from HeLa and rat hippocampal neurons. *A.* Boxplot of the log₂ intensities for the different starting amounts of protein from HeLa showing an increase in intensity and intensity distribution with increasing amount of material *B.* Boxplot of the normalised log₂ intensities for the different starting amounts of protein from HeLa showing a decreased dynamic range for the lower amounts of material. *C.* Boxplot of the log₂ intensities for the different starting amounts of protein from rat primary hippocampal neurons. *D.* Boxplot of the normalised log₂ intensities for the different starting amounts of protein from rat primary hippocampal neurons. *E.* Distribution of the summed intensities of the different protein starting amounts for HeLa showing a relative overrepresentation of the high sum intensities for the small amounts of material. *F.* Distribution of the summed intensities of the different protein starting amounts for rat primary hippocampal neurons showing a relative overrepresentation of the high sum intensities for the small amounts of material.

